We are IntechOpen,
the world's leading publisher of
Open Access books
Built by scientists, for scientists

5,500
Open access books available

136,000
International authors and editors

170M
Downloads

154
Countries delivered to

Our authors are among the

TOP 1%
most cited scientists

12.2%
Contributors from top 500 universities

WEB OF SCIENCE™

Selection of our books indexed in the Book Citation Index
in Web of Science™ Core Collection (BKCI)

Interested in publishing with us?
Contact book.department@intechopen.com

Numbers displayed above are based on latest data collected.
For more information visit www.intechopen.com

Chapter

International Benchmark Activity in the Field of Sodium Fast Reactors

Domenico De Luca, Simone Di Pasquale, Marco Cherubini, Alessandro Petruzzi and Gianni Bruna

Abstract

Global interest in fast reactors has been growing since their inception in 1960 because they can provide efficient, safe, and sustainable energy. Their closed fuel cycle can support long-term nuclear power development as part of the world's future energy mix and decrease the burden of nuclear waste. In addition to current fast reactors construction projects, several countries are engaged in intense R&D and innovation programs for the development of innovative, or Generation IV, fast reactor concepts. Within this framework, NINE is very actively participating in various Coordinated Research Projects (CRPs) organized by the IAEA, aimed at improving Member States' fast reactor analytical simulation capabilities and international qualification through code-to-code comparison, as well as experimental validation on mock-up experiment results of codes currently employed in the field of fast reactors. The first CRP was focused on the benchmark analysis of Experimental Breeder Reactor II (EBR-II) Shutdown Heat Removal Test (SHRT-17), protected loss-of-flow transient, which ended in the 2017 with the publication of the IAEA-TECDOC-1819. In the framework of this project, the NINE Validation Process– developed in the framework of NEMM (NINE Evaluation Model Methodology) – has been proposed and adopted by most of the organizations to support the interpretation of the results calculated by the CRP participants and the understanding of the reasons for differences between the participants' simulation results and the experimental data. A second project regards the CRP focused on benchmark analysis of one of the unprotected passive safety demonstration tests performed at the Fast Flux Test Facility (FFTF), the Loss of Flow Without Scram (LOFWOS) Test #13, started in 2018. A detailed nodalization has been developed by NINE following its nodalization techniques and the NINE validation procedure has been adopted to validate the Simulation Model (SM) against the experimental data of the selected test. The third activity deals with the neutronics benchmark of China Experimental Fast Reactor (CEFR) Start-Up Tests, a CRP proposed by the China Institute of Atomic Energy (CIAE) launched in 2018 the main objective of which is to improve the understanding of the start-up of a SFR and to validate the fast reactor analysis computer codes against CEFR experimental data. A series of start-up tests have been analyzed in this benchmark and NINE also proposed and organized a further work package focused on the sensitivity and uncertainty analysis of the first criticality test. The present chapter intends to summarize the results achieved using the codes currently employed in the field of fast reactor in the framework of international projects and benchmarks in which NINE was involved

and emphasize how the application of developed procedures allows to validate the SM results and validate the computer codes against experimental data.

Keywords: SFR, Benchmark, EBR-II, FFTF, CEFR, M&S tools

1. Introduction

1.1 History, main features, advantages and future of sodium-cooled fast reactors

Since the very beginning of its commercial operation, immediately after the end of the Second World War, nuclear energy has been getting a significant and often increasing part in the production of safe, secure, and economic low carbon electricity.

Innovation has always been - and still is nowadays - a powerful engine for progress in the fields of regulation (also including the trans-national aspects of the emergency management), safety (with a specific care and attention paid to severe accident prevention and mitigation, e.g. through inherent and passive safety features), reliability and efficiency in design and operation (including reliability and independence of control systems), incineration of long-life by-products of the fission-conversion-breeding process, non-proliferation (uselessness of fuel materials for weapon production), environmental impact (to the air, the soil and the water, both in normal operation and in emergency), management of high and low activity wastes, and also in the very sensitive domain of the public-awareness and acceptance, which are the key-issues for the civil nuclear future [1, 2].

This trend has been even more reinforced after the Fukushima events, also accounting for the wide stress test campaign conducted worldwide, as well as the large effort for public information, participation, and inclusion carried-out by International Bodies, Governments, Constructors, Operators, Academia and Research Organizations [3].

Safety has undergone a continuous improvement effort and has been a relevant driving force for progress, improvement as well as research and development in different fields of endeavor for the current GEN III (Generation III) and GEN III+ (Generation III plus) reactor designs, but also for the advanced concept-designs both inside the GIF (Generation IV International Forum) framework and outside, and in complement to it, e.g. with the ever growing interest for the SMRs (Small Modular Reactors), small compact elementary modules, generally sizing from 10MWe to 300MWe, which are designed and engineered along with a modular construction approach enabling to combine them and incrementally extend the power capacity of the overall plant thus offering economy of scale and reducing both capital costs and construction time [4]. Designs with power outputs smaller than 10MWe, often designed for semiautonomous operation, have been referred to as Micro Modular Reactors (MMRs).

Today, facing the high investment needs and the ever increasing costs, the large delays in the licensing process and the construction, the highly expensive financing modes as well as the low public acceptance and sometimes even the fierce opposition of a majority of the population, some developed countries (mainly in the Western Europe, even if Europe in a whole lasts hosting the largest nuclear capacity of the world), have decided to either step out or phase out nuclear energy in a short-medium term.

Nevertheless, nuclear energy still enjoys an increasing and dynamic trend. The Year 2018 has even been a hit as for the installed new nuclear capacity, mainly because the interest for nuclear reactors has widely moved from developed to emergent - developing countries. This trend is to continue and even expand as, according

to current estimations, the installed nuclear capacity should double in the emergent economies within the next 20years. Relying upon a robust industrial capacity, the Russian Federation is today by far the larger exporter/provider of nuclear technology worldwide, and the People Republic of China is on the way to become a future leader in the nuclear field.

In order to allow nuclear power contribute effectively to the solution of the global warming challenge in the future, it shall be necessary: to continuously up-date and improve regulations; to enhance the safety under the guidance of proactive, transparent and independent Safety Authorities; to establish suitable roadmaps providing all the actors in the nuclear field with a medium - long term clear vision, and to reduce overall costs through continuous improvement, harmonization of practices and standardization. But, mostly, it will be worth addressing and providing a long-lasting and sustainable solution to the crucial problem of the long-lived wastes.

Today, the installed nuclear capacity is by far from GEN III reactors, only a few of them belonging to the GEN III+ generation (which includes, e.g., French EPR, American AP-1000, Russian VVER-1000 …), and even less to other concepts. During their operation, such reactors produce, as by-products of the fission-conversion-breeding process, a large quantity of long-lived isotopes, quoted as Actinides and/or Minor Actinides, depending on their features and nature, which contribute to the activity of the spent fuel for thousands of years.

The build-up of such by-products turns-out a major challenge both from the non-proliferation and the waste management viewpoint. Their recycling in the reactor fuel as well as their incineration through suitable strategies will contribute to "close the cycle", i.e., at least theoretically, to bring the spent fuel activity back to a level comparable to the natural earth radiation. The acceptance of the public of further installations of nuclear power plants will strongly depend in the future on this crucial problem.

Fast reactors closed fuel cycle can efficiently and effectively contribute to the solution of the problem decreasing the burden of nuclear waste and supporting long-term nuclear power development as part of the world's future energy mix [5].

Global interest in fast reactors has been growing since their inception in 1960's because they can provide efficient, safe and sustainable energy. In addition to the current fast reactor construction projects underway, several countries are engaged in intense research and development programs for the development of innovative, Gen IV, fast reactor concepts, as proposed by the GIF. They include three fast neutrons concepts: the SFR - Sodium Fast Reactor -, the LFR - Lead (or Lead-Bismuth) Fast Reactor - and the GFR (Gas Fast Reactor), as well as the MSR (Molten Salt Reactor) which can be declined both in a thermal and a fast neutrons version.

Moreover, current developments of SMRs include, among the more than 100 versions under study, development and/or licensing, several fast neutrons concepts, even though the most mature ones are undoubtedly based on LWR (Light Water Reactor) technology. The fast SMRs, in addition to their efficient use of the fuel, are flexible because they can operate either as breeders, to produce fissile material, or as burners of Plutonium and/or long-lived Minor Actinides. Combining this capability with the benefits in terms of power generation flexibility, SMRs could turn-out quite attracting.

The SFR is, by far, the fast reactor technology most widely spread-out worldwide. It enjoys an acknowledged maturity due to the numerous constructions and because it underwent many years of operation in several countries, from the late '60 prototypes up to the development and deployment of the industrial French fleet (including RAPSODIE, Phénix and Superphénix - the biggest fast reactor ever built, now decommissioned -, and the project ASTRID, now delayed), and other reactors now either in operation or under construction in Russia, India, China and Japan (see **Figure 1**).

Figure 1.
World Sodium Fast Reactor Status.

Design and operation of such reactors are demanding extended computation capacity, to assess their safety, security, and economics [6], which justifies the organization under IAEA's umbrella of Coordinated Research Projects (CRPs) aimed at improving Member States' fast reactor analytical simulation capabilities and international qualification through code-to-code comparison, as well as experimental validation on mock-up experiment results of codes currently employed in the field of fast reactors. NINE is very actively participating in these exercises, and sometimes conducting them.

The present chapter summarizes the results and discusses the main outcomes of the above-mentioned benchmark exercises, in the aim at underlying the wide convergence among the computational tools adopted by the participants, as well as detecting the main discrepancies and seeking for their common origin and trend, whether and whenever existing. That should enable defining a mid-term vision for further development of the computer codes in the field of fast reactors, whatever their features and nature, and identifying new needs for their extended validation against either available or expected experimental data.

1.2 NINE involvement/interest in sodium-cooled fast reactors

Starting from the considerations above regarding the deployment of fast reactors and the maturity gained by the SFR, NINE joints the effort of International community to assess the actual computational capabilities in modeling SFRs features. Taking advantage of reactor data gathered in full scale reactor demonstrators, NINE participated, and is still doing, in several International benchmarks aiming at demonstrating the applicability of its modeling methodology to Fast Reactor design and, in particular, to SFRs; to evaluate the level of assessment of computer codes available at NINE in respect to SFR specific features; to check the applicability of the NINE Validation Process – which is part of the more general framework of NEMM (NINE Evaluation Model Methodology)[1] - with particular focus on the quantification of accuracies of the Thermal–Hydraulic (TH) simulations by means of Fast Fourier Transform Based Method (FFTBM) and finally to perform independent validation of the Serpent code.

All the analysis presented hereafter have been performed following a best estimate approach which requires, among the other things, a high-fidelity Simulation

---

[1] Within the NEMM (NINE Evaluation Model Methodology), NINE adopts the conventional and internationally acknowledged process to achieve the validation of computation tools and define the inherent uncertainties. It includes three steps: the analytical compliance test - the verification -, the qualification through code-to-code comparisons and benchmarks, the actual validation – supported by scaling analysis – on experimental data originating from mock-up experiments and the outcomes of the operating experience, including downgraded operation and emergency.

Model (SM), i.e., a SM that represents with a high level of detail the hardware subject of the analysis to avoid the introduction of inaccuracies due to rough approximations and assumptions.

2. Analysis and validation of EBR-II SHRT-17

The IAEA CRP "Benchmark Analyses of EBR-II Shutdown Heat Removal Tests" was initiated in 2012 [7] with the objective of improving the state-of-the-art SFR codes by extending their validation to include comparisons against whole-plant data recorded during landmark Shutdown Heat Removal Tests (SHRT) conducted at Argonne's Experimental Breeder Reactor II (EBR-II) in the 1980's.

The EBR-II plant was a uranium metal-alloy-fuelled liquid-metal-cooled fast reactor designed and operated by Argonne National Laboratory (ANL) for the U.S. Department of Energy at the Argonne-West site.

Several loss of flow tests were conducted in the facility between 1984 and 1986, as a part of SHRT series [8]. SHRT-17, protected loss of flow transient, was one of the mentioned tests to demonstrate the inherent safety of LMR type reactors. At the beginning of the test, the primary pumps were tripped and at the same time a scram was actuated through a full control rod insertion. The effectiveness of natural circulation cooling capability of the reactor, which makes them inherently safe under described accident conditions, was successfully demonstrated by this test.

2.1 The NEMM validation process

2.1.1 Overview of SCCRED methodology

A key feature of the activities performed in the field of nuclear reactor safety is the need to demonstrate the validation level of each tool adopted within an assigned process and of each step of the concerned process. Therefore, the validation of best estimate codes, models, "best modeling practices" and uncertainty methods must be considered of great importance to ensure the validity of performed Best Estimate and Uncertainty analysis. A consistent code assessment supported by a qualified experimental database is an important step for developing a solid ground for the uncertainty evaluation in the frame of Best Estimate and Uncertainty approach. Thus, the SCCRED (Standardized and Consolidated Calculated & Reference Experimental Database) methodology [9], embedded in NEMM [10], has been developed to generate a series of documents and tools to set up a qualified experimental and calculated database for Verification and Validation (V&V) purposes of Best Estimate and Uncertainty applications.

Figure 2 depicts the SCCRED diagram: the information contained in the experimental reports together with the code input nodalization are the sources to be elaborated in a systematic way by a qualified database made up of the following documents:

- The Reference Data Set for the selected facility or test (RDS-facility and RDS-test) containing the information (geometrical data of the facility and boundary and initial conditions of the selected test, respectively) needed for the code input development;

- The Validation Report (VR), which collects the results of the Validation Process of the performed code calculation;

- The Engineering Handbook (EH), that describes the code input file and provides the engineering justifications of the code-user choices.
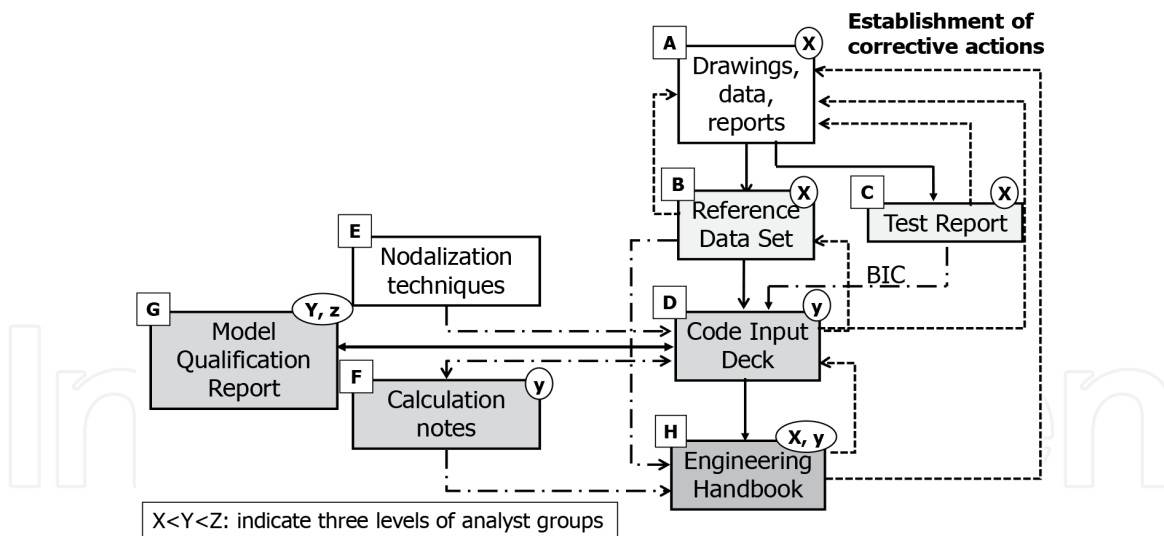
Figure 2.
SCCRED Flow Chart.

The flow-chart linking the RDS, the Input deck, the VR and the EH is high-lighted in **Figure 2**. The solid lines show the time sequence of the activities, the dotted lines indicate the feedback for the review and the dashed lines are the necessary input to develop the input deck and the EH.

2.1.2 The validation procedures

The Validation Process of a thermal–hydraulic system code calculation has the goal to demonstrate that the code results (obtained by the application of the code with the developed nodalization) constitute a realistic approximation of the reference plant behavior (a full-size Nuclear Power Plant or a facility). The flow chart of the adopted Validation Process is given in **Figure 3**.

A SM representing an actual system (ITF or NPP) is qualified when:

• It enjoys a large geometrical fidelity with the involved system;

• It reproduces the measured nominal steady state condition of the system;

• It shows a satisfactory behavior in time dependent conditions.

Based on this, three main phases of the Validation Process can be distinguished:

1. The demonstration of the geometrical fidelity of the developed nodalization;

2. The demonstration of the steady state achievement;

3. The "on-transient" Validation.

In relation to the first step of the methodology it is worth demonstrating that the discrepancies between relevant geometrical parameters of the plant and the data implemented into the nodalization are within acceptable values.

The second step of the Validation Process deals with the achievement of the steady state. A set of significant parameters is identified to demonstrate that the discrepancies between calculated and measured data available from nominal stationary conditions are within acceptability thresholds.
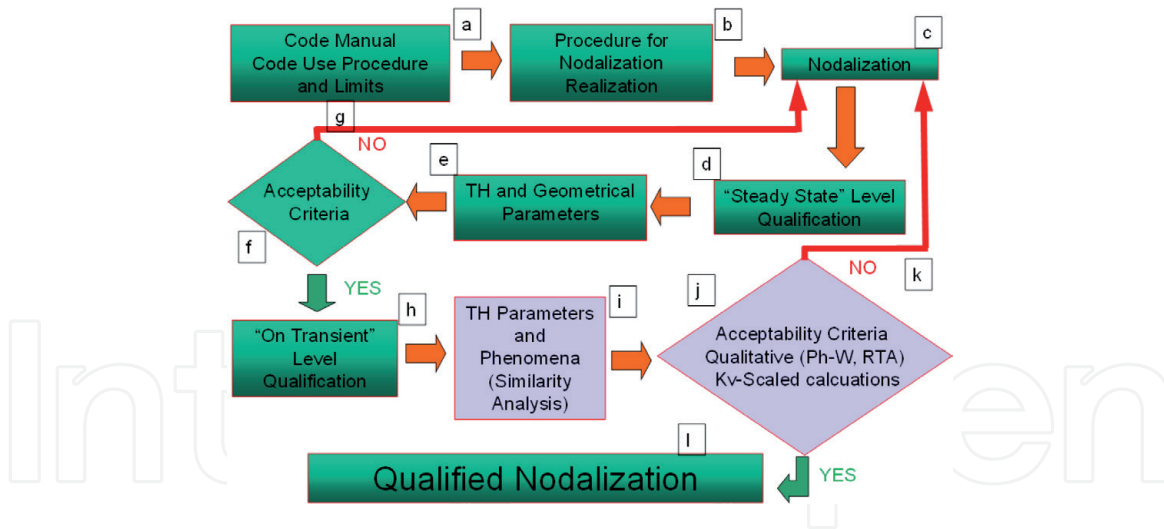
Figure 3.
Flow Chart of the Validation Procedures for the SM.

The third step of the Validation Process is the "On-transient" validation, a very complex step requiring several different sub-steps which include qualitative and quantitative accuracy evaluations performed to evaluate the acceptability of the calculation on "transient level". If the qualitative accuracy evaluation is acceptable, the accuracy of the code calculation can be quantified utilizing the Fast Fourier Transform Based Method (FFTBM) [11].

2.2 EBR-II plant and the developed SM

The EBR-II plant, located in Idaho, was operated by ANL for the U.S. Department of Energy from the beginning of 1964 until 1994. EBR-II rated thermal power was 62.5 MW, with electric output of 20MW. EBR-II was a sodium-cooled reactor fueled with uranium metal alloy fuel, with a pool type primary system. **Figure 4** shows the configuration of the main components in the EBR-II primary system [12] together with the developed RELAP5 SM.

All major primary system components were submerged in the primary tank. Two primary pumps drew sodium from the pool and provided sodium to the two inlet plena for the core, through high pressure and low-pressure pipes. The reactor
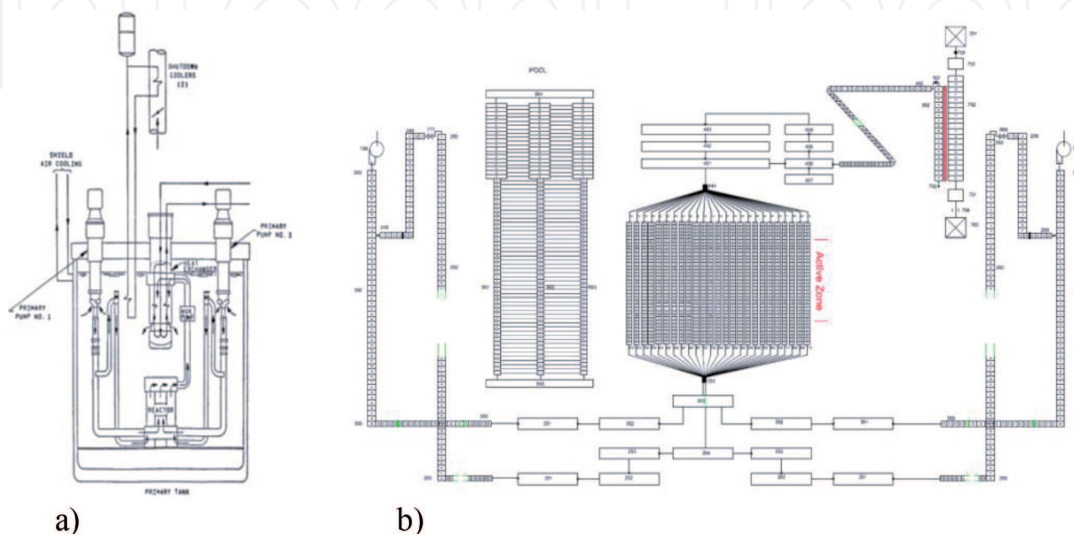

Figure 4.
(a) EBR-II Primary System and (b) The adopted Nodalization.

vessel accommodated 637 hexagonal subassemblies divided in three regions: central core (up to row 5), inner blanket (rows 6 and 7) and outer blanket (up to row 16). Hot sodium exited the subassemblies into a common upper plenum where it mixed before passing through the reactor outlet pipe ("Z-pipe") into the Intermediate Heat Exchanger (IHX). Sodium then exited the IHX into the primary sodium tank before entering sodium primary pumps.

The EBR-II benchmark specifications [12] were used to develop a detailed thermal hydraulic model (see **Figure 4b**) of the reactor. The RELAP5 system thermal hydraulic code was used for both performing the nodalization and running the calculations.

The whole reactor core consisted of 96 channels representing all 10 types of subassemblies used in the reactor, and two bypass flow paths. The reactor vessel was first subdivided into 16 rows. The subassemblies in the first 6 rows have been modeled separately (1 by 1) with 81 channels, except for safety/control rods that have been merged into one channel. Rows 7 to 16 made of reflector and blanket subassemblies have been modeled with one channel per type of subassembly in each row. One heat structure component has been used to simulate the active part of the fuel pins for each subassembly in the central core region, assuming a flat and constant power profile along all the active length. The pool was modeled with a cylindrical multi-dimensional component having 3 azimuthal meshes, two of which were thermally linked to the pumps and the third one to the IHX. The heat exchanger was of counter-current flow type. The primary side of IHX has been modeled with a pipe which takes hot sodium flowing out from the "Z-pipe" and discharges the cold sodium directly into the pool. The intermediate side of IHX has also been modeled with a pipe equivalent to 3026 secondary tubes through which the intermediate sodium flows. The boundary conditions for the intermediate side were imposed by the time-dependent volume and time-dependent junction components.

2.3 Transient results and sensitivity analysis of EBR-II SM

2.3.1 Reference results

The transient was initiated by a trip of primary and intermediate pumps, which instantaneously scrammed the reactor. While the coast-down shapes for SHRT-17 were designed to be identical for the two primary pumps, intrinsic differences between the two pump drive units caused a difference in the stop times.

The transient calculation was performed after the achievement of acceptable steady-state conditions. Starting from full power and flow, both the primary loop and the intermediate loop coolant pumps were simultaneously tripped, and the reactor was scrammed to simulate a protected loss-of-flow accident. Therefore, in the early stage of the pump coast-down (up to about 10 s) the cladding and the outlet coolant temperature decreased. During the transition from the forced to natural circulation (between 10 and 100 s) the mass flow rates decreased rapidly and the unbalance between the total core power and the energy removed from the primary coolant caused a rapid increase of the cladding temperatures and a slower increase of the coolant temperatures. When the natural circulation is fully established (after about 100 s) the total core power is efficiently removed in all subassemblies and the coolant and cladding temperatures decrease.

During the pump coast-down the mass flow rate in the instrumented subassembly XX09 remained a little bit higher than the experimental data (see **Figure 5**), which affected the coolant and cladding temperatures in the whole subassembly. Indeed, both the coolant temperatures below (**Figure 6**) and above (**Figure 7**) the active core region and the cladding temperatures at the middle and at the top of
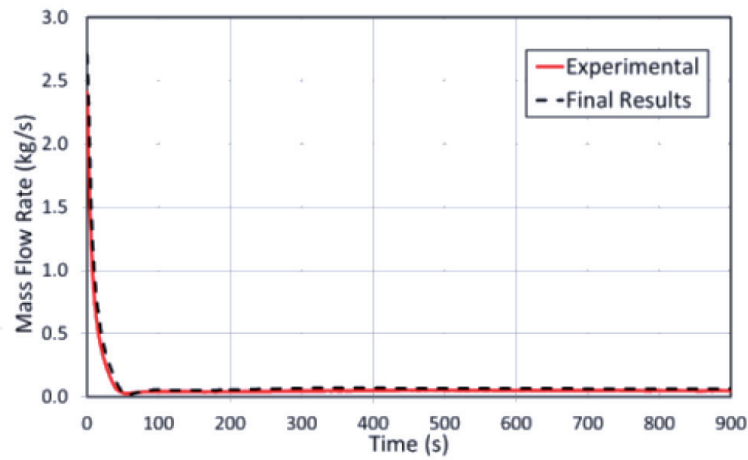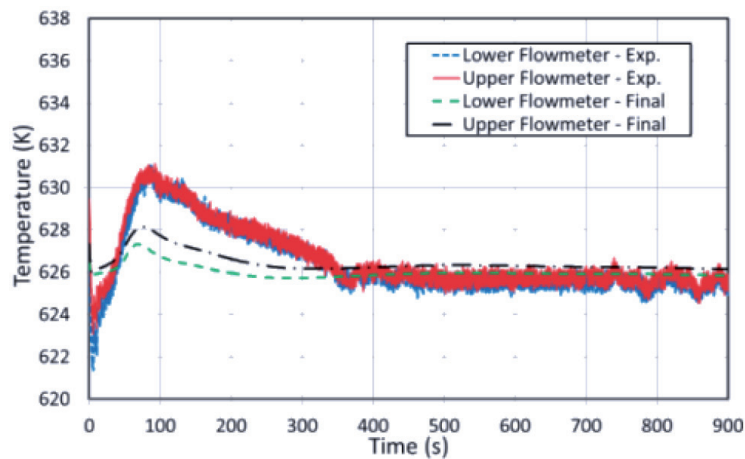
Figure 5.
XX09 Mass Flow Rate.

Figure 6.
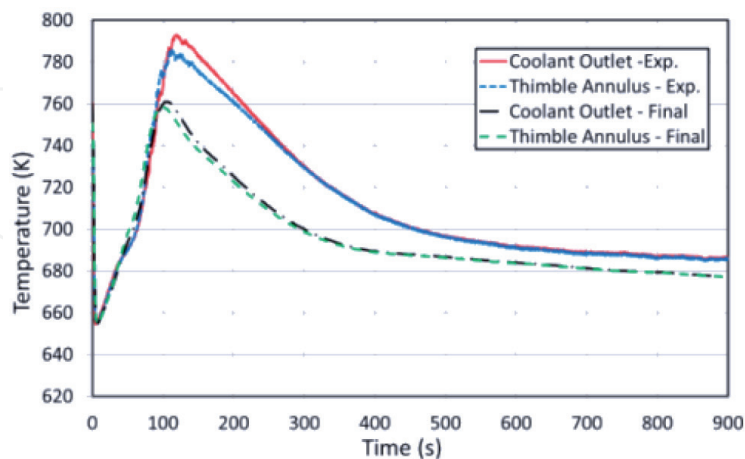*XX09 Lower and Upper Flowmeter Coolant Temperatures.*

Figure 7.
XX09 Outlet and Thimble Annulus Coolant Temperatures.

the core (**Figure 8**) were slightly lower than the experimental data. These small differences became negligible during the long-term cooling because the mass flow rate reached the correct value. It should be noted that the flowmeter temperatures, where the gamma heating occurs, were qualitatively correctly predicted by the simulation.
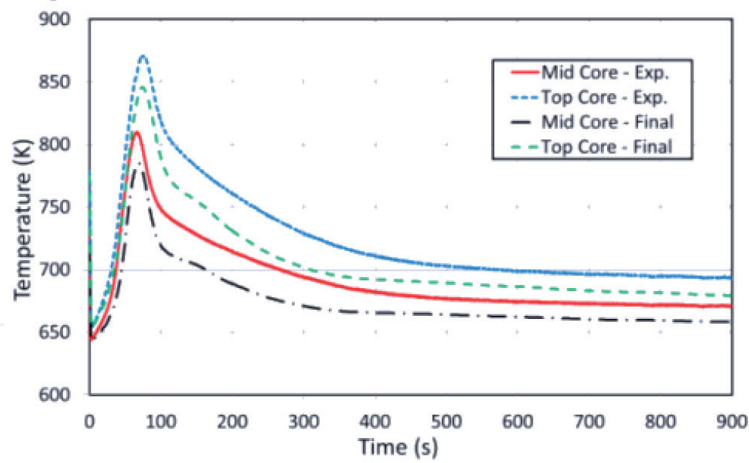
Figure 8.
XX09 Clad Temperatures.

2.3.2 Sensitivity analysis

During the phase 2 of the benchmark, a sensitivity analysis on the gamma heating was performed aimed at understanding the experimental behavior of the coolant temperature at the inlet and outlet of instrumented subassembly (in particular, the instrumented subassembly XX09).

To perform the sensitivity analysis a simple model (see **Figure 9**) of the instrumented subassembly XX09 was developed considering only the subassembly channel and the guide thimble annulus channel, thermally connected with a passive heat structure simulating the subassembly walls. The heat structure simulating the guide thimble wall has been isolated. Regarding the active heat structure, in addition to the flat power profile adopted in the early stage of the phase 2 of benchmark (Phase-2A), four different axial power distribution (see **Figure 9**) have been implemented:

1. Power supplied also below the active part of the core;

2. Power supplied also above the active part of the core;

3. Power supplied also above and below the active part of the core;
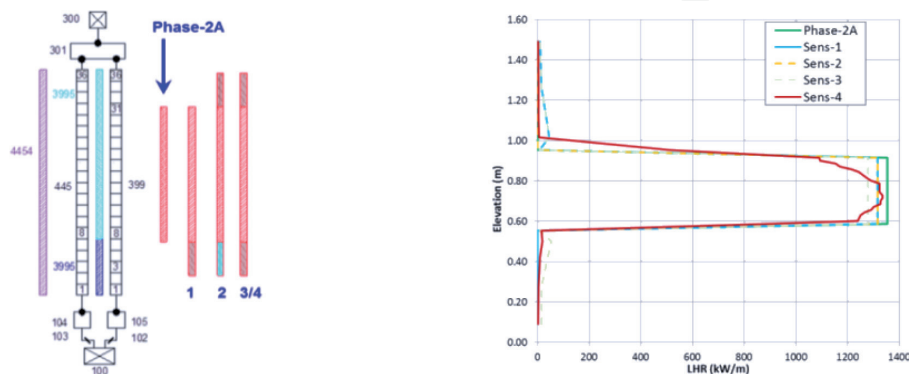
4. Axial power distribution as in SHRT-45.

Figure 9.
XX09 Model and Axial LHR used in the Sensitivity Analysis.

The axial power distribution below the BAF has been calculated to match the experimental steady state values of the coolant temperature at the lower and upper flowmeter thermocouples. It can be noted that the power supplied below the active part of the core (sensitivity #1, 3 and 4) positively affects the temperature trends at the upper flowmeter thermocouples (see **Figure 10**).

On the contrary, the power supplied above the active part of the core (sensitivity #2, 3 and 4) results in minor effect on the temperature trends. In particular, the coolant outlet temperature (see **Figure 11**) shows a light delay in the temperature increase after the pump coastdown compared to the experimental data and to the other sensitivity cases.

2.4 Validation process of the EBR-II SM

In the framework of the benchmark, a simplified version of the Validation Process was adopted selecting a smaller set of parameters to carry-out the demonstration of the geometrical fidelity and the demonstration of the steady state achievement (see §2.1.2). In addition, only a quantitative analysis by the FFTBM was carried-out, without performing the qualitative analysis (which is instead a mandatory step for a full application of the Validation Process) due to limited project's recourses. The main goal of the quantitative evaluation, as well as the analysis carried out, was to support the interpretation of the results calculated by the CRP participants, i.e., to provide quantitative measures of the discrepancies between the assumptions made by the participants and the reference specification data. These discrepancies can provide a support to understand the reasons for the differences between the participants' results and the experimental data. Results from the application of the Validation Process are available in [7].

First, a list of more than 50 parameters was selected to perform the geometrical fidelity between the EBR-II hardware and the developed nodalization.

For the achievement of the steady state, a set of significant parameters was identified to demonstrate that the discrepancies between calculated and measured experimental data were within acceptability thresholds.

Regarding the third step of the Validation Process, the "On-transient" Validation, the focus was only on the so called "Quantitative Accuracy Evaluation" that is performed by the FFTBM. A list of about 50 parameters was selected,
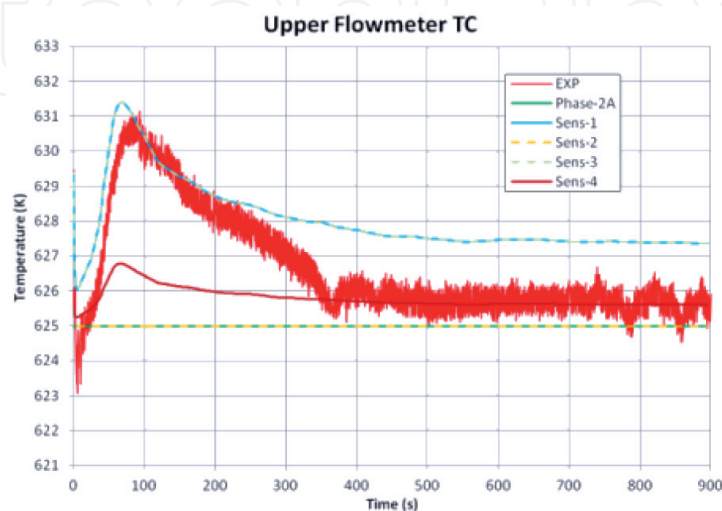

Figure 10.
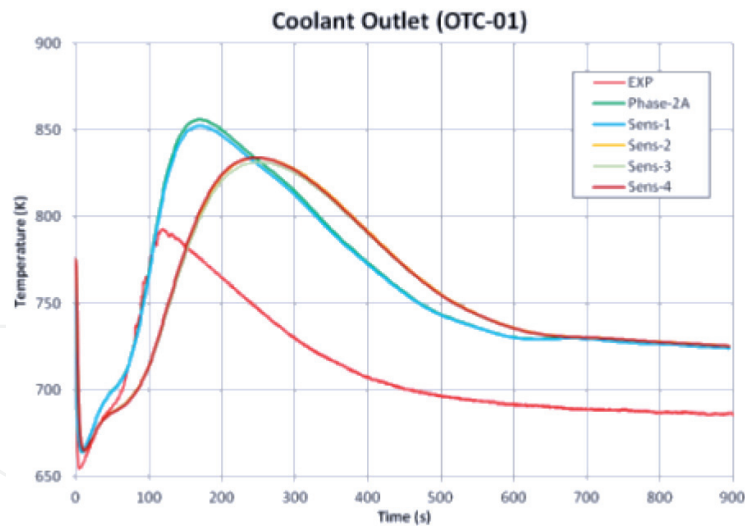*Upper Flowmeter Temperature.*

Figure 11.
Coolant Outlet Temperature.

varying from power, absolute pressures, velocity and mass flow rates, fluid temperatures, rod surface temperatures, pressure drops and mass inventory. In the case of parameters for which no reference or measured value was available a code-to-code comparison was performed.

3. Analysis of FFTF LOFWOS Test #13

The IAEA CRP focused on benchmark analysis of one of the unprotected passive safety demonstration tests performed at the Fast Flux Test Facility (FFTF) was launched in 2018 to support collaborative efforts within international partnerships on the validation of simulation tools and models in the area of sodium fast reactor passive safety.

The Fast Flux Test Facility was a 400 MW-thermal loop type SFR prototype with mixed oxide fuel, built to assist development and testing of advanced fuels and materials for fast breeder reactors. It was located at the Hanford site in Washington and designed by the Westinghouse Electric Corporation for the U.S. Department of Energy (DOE). FFTF reached criticality in 1980 and has been operating until 1992 [13].

The loss of flow without scram (LOFWOS) Test #13 was performed on July 18, 1986 as part of the Passive Safety Testing (PST) program with the aim of confirming the safety margins of FFTF as a liquid metal reactor, providing data for computer code validation, and demonstrating the inherent and passive safety benefits of its specific design features. One of the passive reactivity control devices are the Gas Expansion Modules (GEMs) located at the periphery of the FFTF core. GEMs are hollow tubes sealed at the top and open on the bottom with Argon cover gas trapped inside. During normal operation, the pressure head of the primary pumps compresses the gas to a level above the active part of the core, filling the GEMs with sodium. Following a pump trip and a corresponding decrease in the sodium pressure, the trapped gas would expand and displace sodium, increasing the neutron leakage from the core and decreasing the core reactivity.

Starting from 50% power and 100% flow, the Test #13 was initiated when the three primary sodium pumps were simultaneously tripped. The secondary loop sodium pumps remained operational throughout the whole test.

3.1 Overview of FFTF and of the developed SM

An overview of the FFTF coolant system is shown in **Figure 12**, where three main parts can be distinguished: the reactor vessel, the primary loop, and the secondary loop.

Regarding the reactor vessel, cold sodium was discharged from the three primary loop inlet pipes into an inlet plenum at the bottom of the reactor vessel. Sodium was then drawn up into the core support structure and distributed to the core assemblies and radial shields, as well as leakage and bypass flow paths. Sodium discharged from these flow paths was mixed above a horizontal baffle plate in a common outlet plenum before exiting the reactor vessel through one of three primary loop outlet pipes. The outlet plenum was bounded at the top by a region of Argon cover gas.

The IHX was vertically mounted counterflow shell and tube designs and separated activated sodium coolant in the primary loops from nonradioactive sodium in the secondary loops. Within each secondary loop, hot leg piping ran from the IHX outlet to a Dump Heat Exchanger (DHX) unit, which discharged heat to the environment. Each DHX unit contained four individual sodium-to-air dump heat exchanger modules. The cold leg sodium ran from the DHX unit to a sodium pump, and back to the IHX.

The FFTF core was loaded with199 hexagonal assemblies, that could be grouped in 91 core locations, from row 1 to row 6, including 7 different types of driver fuel assemblies, control and safety rods and test locations, 60 internal reflector assemblies, in rows 7 and 8A, and 48 external reflector assemblies, in rows 8B and 9.

Starting from the benchmark specifications [13], a detailed SM reproducing each component depicted in **Figure 12** was developed following the NINE nodalization techniques, except for the DHXs, that were replaced by boundary conditions.

The reactor vessel has been modeled with a cylindrical multi-dimensional component having three radial meshes: the innermost region represents the area occupied by the core basket and the leakage flow that passes around the fuel assemblies and reflector assemblies (up to row 8A), the intermediate zone models the annular plenum and the flow around reflector assemblies (rows 8B and 9) and through radial shields, and the outermost region simulates the peripheral plenum and the in-vessel storage region. The flow through the assemblies in the reactor core was modeled with 18 channels, 16 pipe components simulating the sixteen assembly flow zones representing the different types of assemblies and 2 pipe components to simulate separately the instrumented assemblies, the Row 2 fast response Proximity
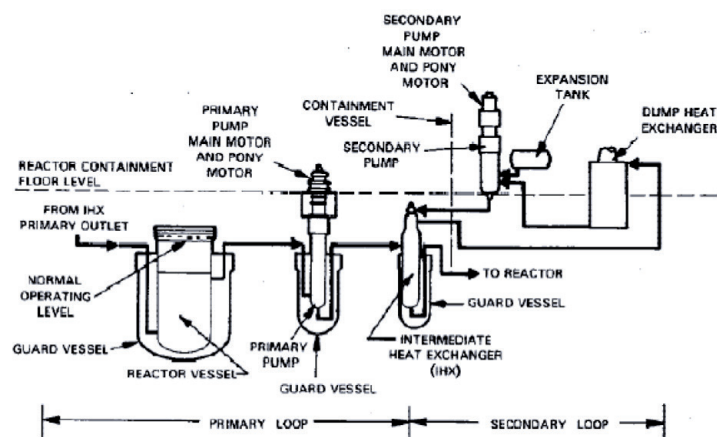

Figure 12.
FFTF Coolant System Overview.

Instrumented Open Test Assemblies (PIOTA) and the Row 6 fast response PIOTA. As for the hydraulic part, one heat structure was inserted in each channel to simulate the active part of the assemblies. A flat axial power profile was imposed along the active length of all the assemblies.

The three primary loops and secondary loops were modeled separately, each one having the same number of hydraulic components. Regarding the secondary loops, two time-dependent components were inserted to provide the proper boundary conditions, one component at the exit of the hot leg piping to set the secondary side pressure, and one component at the beginning of the cold leg piping, downstream the DHXs, to set the appropriate sodium temperature.

3.2 Reference results and sensitivity analysis of the FFTF SM

After imposing the boundary conditions (i.e., pumps speed, core power and secondary loops flow conditions) provided by the benchmark team, acceptable steady-state conditions were achieved before performing the transient simulation. The RELAP5 system thermal hydraulic code was used to make the analysis.

The FFTF LOFWOS Test #13 was initiated when the primary pumps tripped simultaneously. The row 2 PIOTA outlet temperature shown in **Figure 13** can be observed to describe the behavior of the FFTF core during the transient.

The initial rapid rise of the PIOTA outlet temperature was caused by the increasing core power-to-flow ratio following the pump trips. The outlet temperature peaked at around 10 seconds when the power-to-flow ratio reached its maximum value. Then, the increase in core temperatures together with the drop of the GEM sodium level introduced a large negative reactivity feedback, so power decreased faster than the primary flow rate. The drop in reactor power was quick enough to compensate for the reduced flow rate in the primary loop and the sodium temperature started to decrease. As the GEM sodium level approached the bottom of the core, the negative reactivity insertion slowed down. The core outlet temperature began to rise again, and a second peak occurred when the natural circulation was established. Natural circulation was maintained while power continued to decrease resulting in a decrease of the core outlet temperature until the end of the test.

Figure 13 shows the comparison of the PIOTA outlet temperature predicted by the SM against the measurement (in this and subsequent figures the solid line shows the experimental data while the dashed line displays the SM results). The SM results are in good agreement with the experimental data for the entire duration of
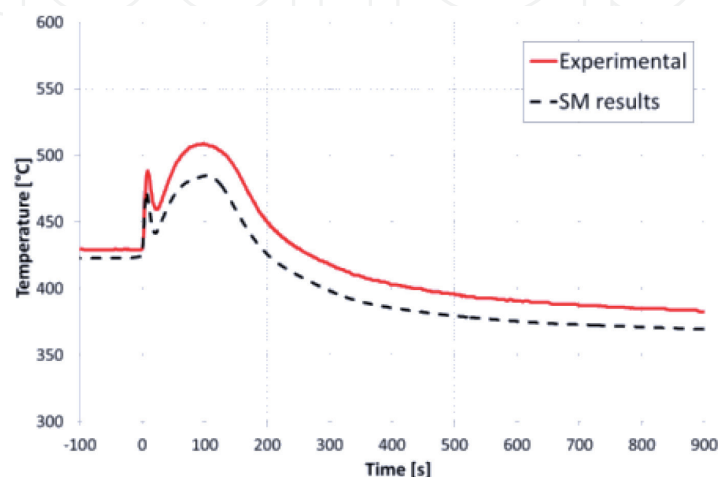

Figure 13.
Row2 PIOTA Outlet Temperature.

the transient. In particular, the time of occurrence of the two peaks is captured very well by the simulation.

The cold leg and hot leg temperatures in one of the primary loops are shown in **Figure 14**. The hot leg fluid temperature has been quite well predicted by the SM, showing a trend slightly oscillating around the experimental value. That may be due to a.

different prediction of the sodium mixing and thermal stratification phenomena in the outlet plenum of the reactor vessel during the natural circulation phase that are difficult to simulate by a system thermal–hydraulic code. The calculated cold leg fluid temperature showed a faster rise at the beginning of the transient following the increase in the DHX sodium outlet temperatures, it reached a higher peak value and it decreased faster compared to the experimental trend. In addition, it can be noted that the oscillations shown in the calculated time trend occurred about 30 seconds earlier and with a greater amplitude than the experimental data. Similar behavior can be observed in **Figure 15**, where the cold leg and the hot leg temperatures in one of the secondary loops are displayed. The cold leg temperature followed the time trends of the DHX sodium outlet temperatures, which had been specified as boundary conditions. The hot leg temperatures decreased quickly at the beginning of the transient reaching the cold leg temperature in about 200 seconds due to the reduction in heat transferred from the primary to the secondary systems across the IHXs, as the primary loop flow rates decreased, and the secondary pumps remained at full speed. It can be noted that, also in this case, the fluctuations of the SM results occur earlier than the measured data.

A sensitivity simulation to account for the thermal inertia of the temperature instrumentation has been performed to investigate the origin of the discrepancies between the SM results and the experimental data. Beyond the reactor vessel, sodium temperatures were measured in the hot and cold legs of all primary and secondary loops by the Resistance Temperature Detectors (RTDs). The RTDs were spring loaded against the bottom of a thermowell to provide a short response time. Unfortunately, there is no information in the benchmark specifications on the geometry of the temperature detectors, so, after a quick search in the literature and some assumptions, a cylindrical heat structure of 5 cm in diameter was inserted at each RTD location. The sodium temperatures detected by the heat structures are shown in **Figure 14** and **Figure 15** (dotted lines) for the primary loop and secondary loop, respectively. When considering the thermal inertia of the RTDs, the SM
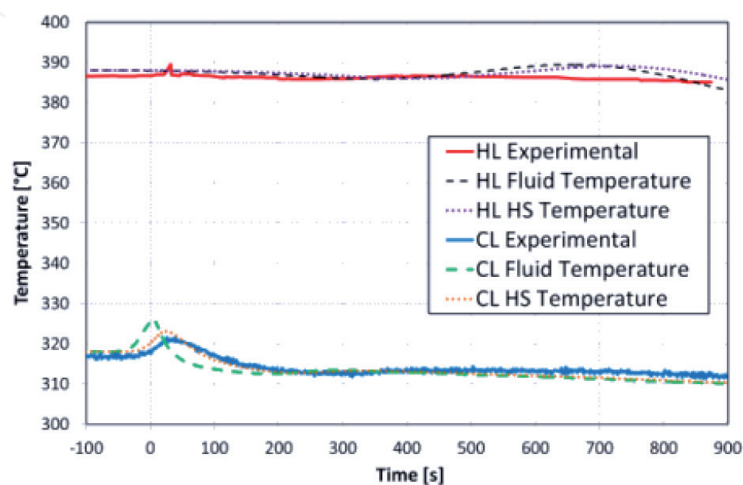

Figure 14.
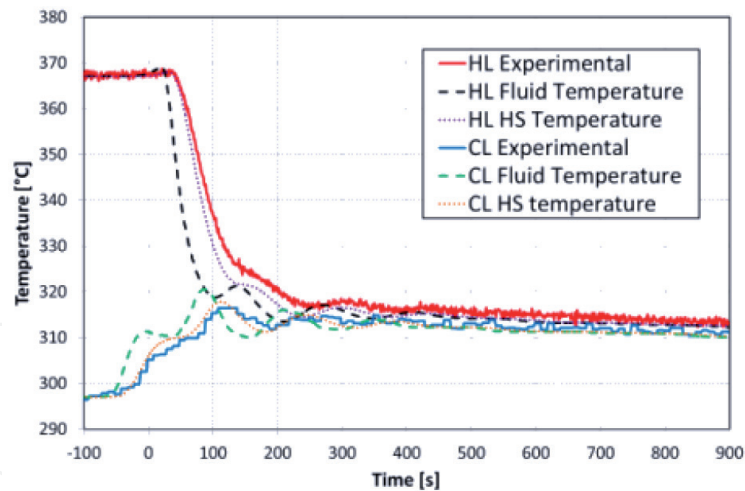*Primary Loop Hot and Cold Leg Temperatures.*

Figure 15.
Secondary Loop Hot and Cold Leg Temperatures.

results are in a very good agreement with the experimental data, improving both the timing and the amplitude of the temperature oscillations.

Then, an additional sensitivity simulation was performed to study the effect of the modeling choice made for the reactor vessel outlet plenum and its impact on sodium mixing. As mentioned before, in the reference case, the reactor vessel and the upper plenum were modeled with a cylindrical multi-dimensional component having three radial meshes. In the two sensitivity simulations, the 3D volumes of the upper plenum were replaced by a 1D vertical pipe component in the first simulation and by a 1D single-volume component in the second simulation. **Figure 16** shows the comparison of the sodium temperature in the hot leg primary loop #1 among the three different reactor vessel outlet plenum modeling choices and with the experimental data. In the reference case (3D) thermal stratification occurs with the hot sodium that tends to go upwards (it should be remembered that the hot leg connection is at the bottom of the outlet plenum, just above the core outlet). In the first sensitivity (1D PIPE), no thermal stratification is observed and the hot sodium exiting the core does not mix with the upper cold sodium at the triggering of natural circulation. In the second sensitivity (1D Single Volume) the hot sodium that would be deposited on top of the reactor completely mixes with the core outlet flow, thus resulting in a slightly higher sodium temperature in the hot leg after the beginning of the transient, compared to the reference case, and which continues to gradually increase even during natural circulation.
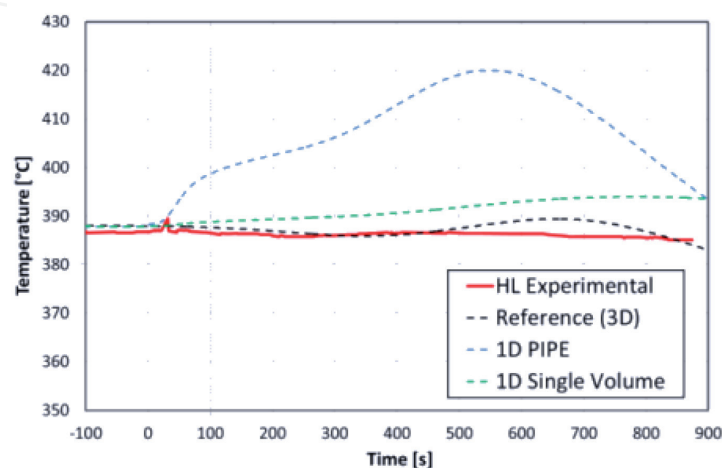

Figure 16.
Sensitivity on Upper Plenum Modeling: Comparison of Primary Loop Hot Leg Temperature.

4. Simulation of the CEFR Start-UP Tests with the Serpent Code

The Neutronics Benchmark of CEFR Start-Up Tests is a CRP proposed by the China Institute of Atomic Energy (CIAE), under the direction and support from IAEA. The CRP was launched in 2018. The main objective of this benchmark is to improve the understanding of the start-up of a SFR and validate the fast reactor analysis computer codes against experimental data obtained at the China Experimental Fast Reactor (CEFR). The CEFR is the first Chinese fast reactor; it is a pool-type sodium cooled reactor, with a nominal thermal power of 65 MWth [14].

NINE, in collaboration with University of Pisa, participated in all the proposed work packages and, in turn, proposed and organized a work package focused on sensitivity and uncertainty analysis of the first criticality test, that, for the time being, has just begun.

The tests included in this benchmark were part of the reactor start-up tests, which included both the fuel loading and the first criticality, the control rod worth measurement, the reactivity coefficients measurement, and the foil activation analysis. All the details of these tests are reported in the Technical specifications [14]. In this chapter, only a sub-set of these tests are analyzed, and their results are compared to experimental measurements.

The first test described is the one referred to the "Fuel loading and criticality" (here and after called work-package 1, WP1). It is focused on the analysis of the first criticality achievement; the tests performed are composed by ten sub-critical steps, with different number of fuel Sub-Assemblies (SAs) loaded, and 3 super-critical steps, which have different RE2 control SA insertion levels. The critical RE2 position was found and reported in the Technical Specification through an extrapolation of the experimental super-critical steps. In this work the results for the super-critical steps, as well as the critical ones, are compared with the experimental measurement; a comparison between two different nuclear libraries is also reported, to exploit the dependence on the nuclear data of the effective multiplication factor.

The second test analyzed is the "Control rod worth measurement", (work-package 2, WP2). The main goal of this test is to evaluate the control rod worth of each control rod SA and of different group of control rod SAs. Also, in this case a comparison with the experimental measurement is reported in the following sections.

The last test presented is the "Foil activation measurements" (work-package 6, WP6): it concerns the foil activation analysis made through the irradiation of different material samples inside the reactor core in both the axial and radial directions.

4.1 The simulation models developed for CEFR

The core geometry has been modeled in its full 3D configuration keeping the heterogeneity of most of the present structures (e.g., the hollowed pellet geometry has been modeled). The SAs model starts from the region above the nozzle (the nozzle is not modeled) and reaches the corresponding head. Only few regions of the core, considered less relevant for the simulations, have been homogenized for the sake of simplification (e.g., SAs Handling head, Spring, etc.). The spacer wires have been homogenized with the corresponding cladding, to guarantee the conservation of the stainless-steel mass. **Figure 17(a)** shows the horizontal section of the core taken at a height of 105.1 cm from the bottom; the operation layout is shown, with all the fuel SAs already loaded in the core. **Figure 17(b)** shows a vertical section crossing the center of the core, along the x axis: the homogenized components are noticeable, mostly on the upper part of each assembly.
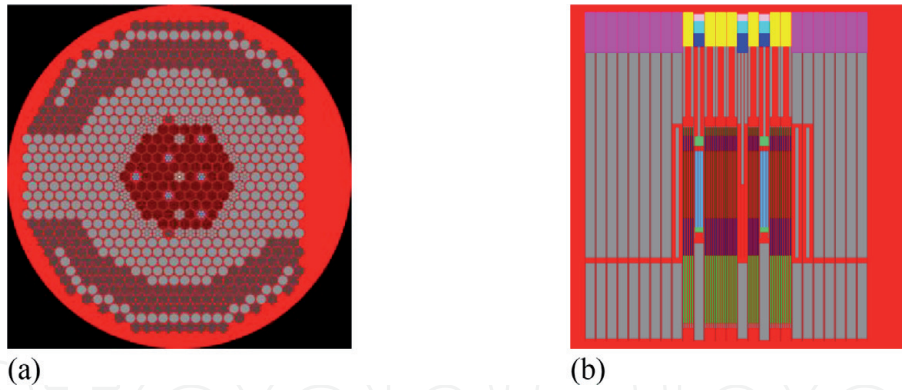
Figure 17.
Serpent Geometrical Core Model: (a) Horizontal Section; (b) Vertical Section.

The Serpent 2.1.31 code [15] was used for all simulations. The ACE format cross-section libraries used have been processed at different temperatures, to match the specification of the various experiment. For the Work Packages (WPs) analysed in this work the data made available by SCK-CEN were used. All the used libraries were based on ENDF/B-VIII.0 [16]; a comparison with the library based on ENDF/B-VII.1 [17] has been performed for one test case of WP1 and has been reported in the following section.

For each experiment, both whole core geometry and material densities have been adjusted to the experimental temperatures, to consider expansion effects, and, therefore, the leakage variation. For most of the materials involved, the temperature adjusted parameters have been determined making use of the linear thermal expansion coefficients. For the sodium coolant density, the correlation provided in the technical specification has been used, while for the Helium gas, the density has been evaluated dividing the mass of gas at cold condition (at 20°C) by the fuel rods free volume available after the expansion (at hot zero power temperature) of the surrounding materials.

For all the experiments, which require a multiplication factor, the Serpent implicit k effective has been considered. In **Table 1** the cycle population, as well as the number of active and inactive cycles are reported.

For each experiment, both whole core geometry and material densities have been adjusted to the experimental temperatures, to consider expansion effects, and, therefore, the leakage variation. For most of the materials involved, the temperature adjusted parameters have been determined making use of the linear thermal expansion coefficients. For the sodium coolant density, the correlation provided in the technical specification has been used, while for the Helium gas, the density has been evaluated dividing the mass of gas at cold condition (at 20 °C) by the fuel

WP	Test cases	Particles number per cycle	Active cycle	Inactive cycle
1	All	5.0E+05	500	50
2	SH and SA	5.0E+05	500	50
	RE	1.0E+06	500	50
6	Axial: U-238, Al-27, U-235, Np-237, Ni-58	2.0E+06	500	50
	Axial: Au-197	4.0E+06		

Table 1.
Simulations Set-up.

rods free volume available after the expansion (at hot zero power temperature) of the surrounding materials. For all the experiments, which require a multiplication factor, the Serpent implicit k effective has been considered. In **Table 1** the cycle population, as well as the number of active and inactive cycles are reported.

4.2 Simulation results and preliminary interpretation of the CEFR SMs

The results presented here are taken from [18]. First, the results of WP1 are analysed. **Table 2** shows the comparison between the calculated and measured values of the effective multiplication factor for the three supercritical steps and the critical position. The relative errors are small and practically constants for all the cases when ENDF/B-VIII.0 nuclear data are used, that suggests a systematic error originating from the nuclear data library can hold. Confirming this, a much better agreement is obtained when use is made of the ENDF/B-VII.1 nuclear data, as the error drops from 0.19% to 0.03% in the case of the RE2 positioned at 190 mm.

Secondly the results of WP2 are presented. **Figure 18** shows the comparison between the calculated and measured integral worth of different control rod SAs, of the two-shutdown system (groups of control rod SAs, considered both fully

# of fuel SAs loaded	Rod position	Serpent output		Experimental	Relative error
	RE2 [mm]	keff	Std. Dev.	keff,exp	$\left\| k_{eff,exp} - k_{eff} \right\| / k_{eff,exp} * 100$
72	70	0.99817	6.00E-05	1.000000	0.18%
72	151	0.99837	6.10E-05	1.000245	0.19%
72	170	0.99848	6.50E-05	1.000335	0.19%
72	190	0.99854	6.00E-05	1.000395	0.19%
72	190 (ENDF/B-VII.1)	1.00072	6.30E-05		0.03%

Table 2.
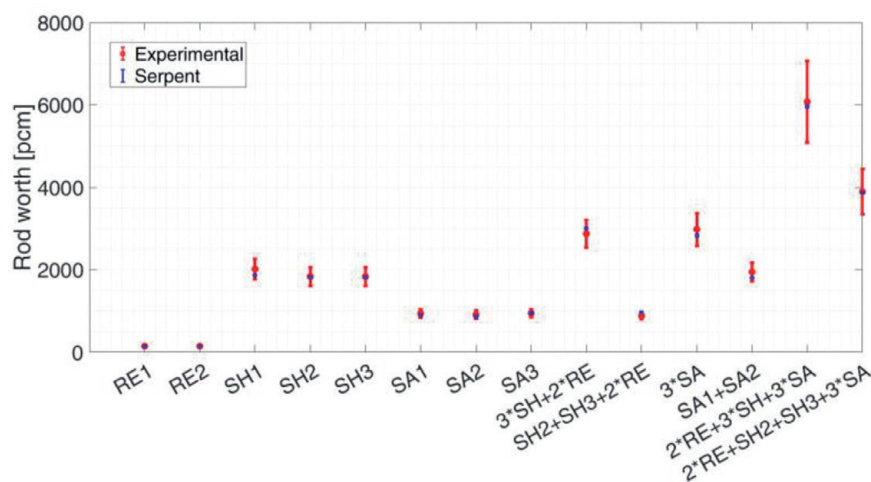*WP1, Comparison with Experimental Data.*

Figure 18.
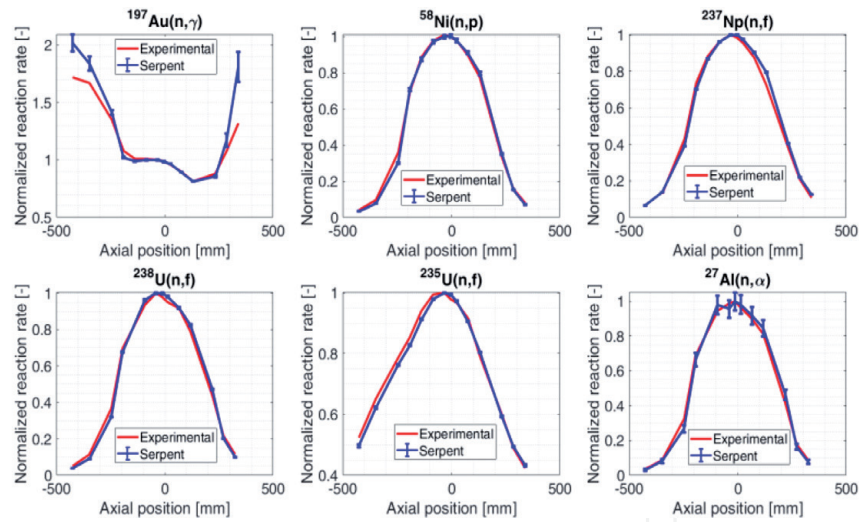*WP2, Comparison with Experimental Data, Rod Worth.*

Figure 19.
WP6, Comparison with Experimental Measurements, Axial Reaction Rates.

operating or with one SA stuck) and of all control rods together. The experimental values are obtained through a rod drop experiment. It appears from the figure that a noticeable good agreement between results and measurements has been achieved.

The last results belong to WP6. In **Figure 19** is reported the comparison between the reaction rates axial distributions evaluated with Serpent and the measured values. The agreement between measurements and simulations is generally quite good. Only the case of ^{197}Au(n,γ) shows a noticeable difference particularly for the positions at the top and bottom of the core. Further investigating and understanding the origin and nature of this discrepancy would contribute to a better understanding of the of the measured activity.

5. Challenges and opportunities for enhanced computation capacity and extended investigation in the sodium-cooled fast reactors field

The core of SFR is subdivided into several hexagonal fuel bundles. Unlike LWR squared subassemblies, these hexagonal subassemblies are compact in size leading to higher power density. Higher power densities and higher coolant temperature can lead to coolant boiling. Besides the difference between the boiling points of the two coolants, a relevant distinguishing feature of sodium is its higher thermal conductivity. While the conduction in water is usually neglected when modeling LWRs, the heat conduction in sodium cannot be ignored in SFRs, mainly when natural circulation occurs. The difference in opacity between the two coolants, also implies adoption of different surveillance methods and the differences in the activation products lead to specific features of shielding (these topics are only mentioned here without deepening because they fall out the scope of this chapter).

Moreover, while LWRs systematically use uranium-oxide fuel (UO2), SFRs can use both oxide and metallic fuel, depending on the design features. The oxide fuel has the advantage of having a high melting temperature relative to the metallic. It is also less ductile and have higher strength. The prediction of the temperature distribution in fuel assemblies should be accurate to assure the safety and reliability of the reactor operation. The focus of the new codes and modeling will be on enhancements to the thermal hydraulics modeling aspects of the SFR and the modeling of metallic fuel.

Another key difference between the designs of Pressurized Water Reactors (PWRs) and SFRs is the structural support of the fuel. While the PWR fuel is supported by grid spacers that are located at specific heights, the SFR fuel is supported by wire-wrappings that extend along the whole length of the fuel. The wire wrapping brings the advantage of a better coolant flow mixing and a lower temperature gradient across the subassemblies, but that comes at the expense of higher pressure-losses along the of the fuel height.

Accounting for the above-mentioned general considerations and trends as well as of the outcomes of the investigations carried-out in the framework of the Benchmark exercises described here above, in paragraphs 2 to 4, the Participants were able to drive some general conclusions on the expected new features of the computation tools as well as on the up-dated methodologies to be adopted for the design and the safety assessment of the Sodium Fast Reactors.

These conclusions identify the main trends for improvement. They can either contribute to further and proficiently expanding the computation capacity of existing tools (and even considering the development of new ones), as well as adapting and/or updating the methodologies adopted so far in the studies.

Moreover, the importance of the representativeness, exhaustiveness and comprehensiveness of the data stored in the data base adopted for validation of the computation tools have been once more and even farther pointed-out. Accordingly, it is considered worth complementing and/or implementing the existing data base with the results of ad-hoc experimental programs, accurately designed, and engineered to match some specific validation needs, thus addressing, and filling the main and more crucial knowledge gaps. Definition of such experimental programs should be made relying upon accurate investigation adopting, e.g., Kriging-like methodologies to avoid duplication and dispersions.

The main topics found-out to be potential levers for further improvement in the SFR computation capacity and reliability are the following:

- A major need for the SFR M&S (Modelling and Simulation) appears to be the improvement of the calculation of inlet-plenum flow distribution and of lateral mixing of coolant flows in the assembly to reduce conservatism in the estimation of the peak fuel and cladding temperatures [19]. The high-fidelity Computational Fluid Dynamics (CFD) models should be developed, tested, and adapted for application to liquid sodium for the relevant flow characteristics and geometric configurations, especially wire-wrapped pin bundles contained within the hexagonal assembly boxes. Additional near-term needs for the SFR M&S are related to the thermal-mechanical modeling capabilities. Recent advances in modeling of oxide fuels behavior in thermal reactors (e.g., fuel and clad conductivity and gap conductance modeling) should also be adapted for fast reactor applications.

- The pressure drop and flow distribution estimation during the transients can be significantly improved when using suitable empiric correlations to model friction losses in the wire-wrapped fuel bundle region, as proposed by Cheng & Todreas [20] and Pontier [21].

- The sodium mixing and the thermal stratification phenomena play a crucial role during the transients, mainly during the natural circulation phase. They cannot be accurately predicted by the current existing SYS-TH (System Thermal–Hydraulic) codes. In addition, these phenomena are also sensitive to the nodalization scheme adopted in the calculations. It is suggested to address this major issue for design and operation through either suitable sensitivity analyses or more in-depth investigations (i.e., adopting CFD codes).

- SFRs use fuel pins tightly packed in a hexagonal duct. As said, to maintain a gap for coolant to flow through, fuel pins are separated with a metallic helical wire spacer wrapped around the pin entire length. Additionally, these wraps mitigate vortex-induced vibration and increase convective heat transfer by enhancing sub-channel mixing. Modeling the flow in wire-wrapped rod bundles is still a challenging problem [22]. Large uncertainties exist in the treatment of wire spacers and drag models used for momentum transfer in current low- resolution (lumped parameter) models. Sub-channel codes apply "forcing functions" to model wrap induced flow mixing. However, these approaches are limited to conditions submitted to a specific validation (flow regime, channel geometry, or operating conditions) and rely on complex coefficients which were derived from fitting the experimental databases the models are based on. High fidelity tools such as CFD can simulate wire-wrapped rod bundles with more detailed resolution. However, CFD simulations are still limited in their capability to characterize long-term transients or large system simulations. They are also bounded by the quality and resolution of the experimental data these models are benchmarked against.

- The axial power profile and the gamma heating outside the core region, below and above the active fuel zone, affect the coolant temperature distribution. That way, they can have a significant impact on the behavior of some transients. In addition, approximations adopted in the calculation of the radial power distribution can engender large computation vs. measurement discrepancies for both dummy and reflector subassemblies (non-fuelled SAs). Accurately account for the gamma heating contribution to the power both in the active and non-active reactor regions can help to correctly address the issue, thus improving the quality of computation results.

- The axial conduction heat transfer modelling is generally either non available or quite poor in the current SYS-TH codes. Even if the contribution of the axial heat conduction with respect to the other heat transfer mechanisms is always negligible in fast systems, accounting for the phenomenon in the heat structures improves the simulation results for the coolant temperature distribution outside the core region, while it does not provide any measurable gain for the evaluation of the cladding temperature, and even, sometimes it turns-out damaging. No specific action is recommended on this issue.

- The correct and comprehensive simulation of the heat transfer between adjacent subassemblies is mandatory to improve the agreement between computation results and measured data. Accounting for radial heat transfer with neighboring subassemblies is mandatory to obtaining good coolant temperature predictions. Accordingly, it is recommended to accurately account for the heat transfer between adjacent subassemblies and developing the suitable computation capacity to do.

- From a pure phenomenological point of view, the transport codes can catch all the phenomena included in the libraries. Nevertheless, data in the libraries have not got the same accuracy level for all phenomena, that can propagate discrepancies to the results. Accordingly, it is strongly recommended to carry-out sensitivity and uncertainty analysis on the nuclear data, when estimated necessary.

- The cross section pre-processing routine implemented in some codes, such as the Doppler-broadening pre-processor routine inside Serpent 2, are not able to adjust the temperature of the unresolved region probability tables. According to the importance of that region for the stability and operability of the core, when using such codes for fast reactor systems, it is recommended to evaluate the Doppler broadening with a suitable nuclear data processing code.

- When using Monte-Carlo codes, the calculation time to achieve a good statistic can turn-out remarkably high. This issue being in common with all Monte Carlo calculations and not being a specific problem for the Sodium Fast Reactor simulation, no specific recommendation is done.

- Many experiments have been performed to study thermal- hydraulics characteristics, primarily pressure drops, of the wire-wrapped fuel bundles. Often however, the uncertainties of pressure drop measurements associated with these experiments is high due to the geometrical complexity of the hexagonal wire-wrapped fuel bundle. Recently [23, 24], a database of pressure drops and flow-field measurements in a 61-pin wire-wrapped hexagonal fuel bundle was developed with the sole purpose to benchmark the existing correlations and validate the CFD calculations. These experiments investigate the flow characteristics in the near-wall region of the 61- pin wire-wrapped hexagon fuel bundle.

All the above-mentioned topics merit for careful consideration and further investigation in view of the definition of future R&D programs in support to the industrial development and the deployment of the SFRs. Due to their size and scope, they should mainly be addressed in the framework of international collaborations.

6. Conclusions

Sodium Fast Reactors is a branch of Fast Reactors technology developed since the early 60s, which nowadays regains large interest and attractiveness thanks to their flexibility and their potential to be operated as Actinide burners and/or breeders, thus playing a crucial role in the closure of nuclear fuel cycle and solving the burden of long-lived nuclear wastes.

Design and operation of such reactors require a noticeable computational capacity, but also specific means to assess their safety both in normal and downgraded operation as well as in emergency conditions. In this prospect, IAEA has organized several Coordinated Research Projects aimed at improving Member States' fast reactor analytical simulation capabilities.

The participation in such research programs - allowing direct comparison of computation results with measured data - contributes to increase the confidence in the capabilities of available computational tool, in the meantime highlighting the potential for improvements which could address and solve the pending issues and for the identification of new ones.

NINE has been actively involved in such research activities within the IAEA CRPs, thus catching the opportunity to independently assess and validate several commonly and widely used Thermal–Hydraulic and Reactor Physic codes. Moreover, it contributed to the comparison of results and the interpretation of discrepancy origins, identifying trends, and driving conclusions for future developments.

The NINE's Simulation Models have been developed strictly complying with the Best Estimate principle - which namely requires avoiding the introduction of inaccuracies due to rough approximations and assumptions - thus trying to represent at best the problem under investigation without adopting any major simplification. Despite this approach requires relevant and continuous computational efforts, the obtained results show-up highly satisfactory and encouraging in a whole. Moreover, as far as the computation capacity is concerned, the NEMM model methodology developed by NINE confirmed its applicability also in the case of SFR simulations.

The present chapter summarizes the activity carried-out, presents the results and discusses the main outcomes of the mentioned benchmark exercises, underlying the wide convergence among the computational tools, as well as detecting the main discrepancies and seeking for their common origin and trends, which should enable defining a mid-term vision for further development of the computer codes in the field of fast reactors and identifying new needs for their extended validation against either available or expected experimental data.

Among others, the following items have been identified as meriting careful and particular attention in the future: the need for an accurate modelling of the mixing of coolant flows in the assembly, the estimation of the pressure drop and the flow distribution during the transients which could be significantly improved using suitable empiric correlations, the sodium mixing and the thermal stratification phenomena which play a crucial role during the transients, and are sensitive to the nodalization scheme adopted and cannot be accurately predicted by the current existing SYS-TH codes, the need for a correct and comprehensive simulation of the heat transfer between adjacent subassemblies, the suitability for improvement of the calculation of inlet-plenum flow distribution.

Moreover, the importance of the representativeness, exhaustiveness and comprehensiveness of data have been once more and even farther pointed-out, claiming the need for complementing and/or implementing the existing data base with the results of experimental programs, engineered to match some specific validation needs, thus addressing, and filling the main and more crucial knowledge gaps. Definition of such programs should rely upon accurate to avoid duplication and dispersions.

Acknowledgements

Glossary

ANL	Argonne National Laboratory
CEFR	China Experimental Fast Reactor
CFD	Computational Fluid Dynamics
CIAE	China Institute of Atomic Energy
CRP	IAEA Coordinated Research Project
DOE (US)	Department of Energy
DHX	Dump Heat Exchanger
EBR-II	Experimental Breeder Reactor II
FFTBM	Fast Fourier Transform Based Method

FFTF	Fast Flux Test Facility
GEN III	Generation III
GEN IV	Generation IV
GEM	Gas Expansion Module
GFR	Gas Fast Reactor
GIF	Generation IV International Forum
IAEA	International Atomic Energy Agency
IHX	Intermediate Heat Exchanger
ITF	Integral Test Facility
LFR	Lead (or Lead-Bismuth) Fast Reactor
LOFWOS	Loss of Flow Without Scram
LWR	Light Water Reactor
MMR	Micro Modular Reactor
MSR	Molten Salt Reactor
NEMM	NINE Evaluation Model Methodology
M&S	Modelling and Simulation
NPP	Nuclear Power Plant
PST	Passive Safety Testing
PWR	Pressurized Water Reactor
R&D	Research and Development
RDS	Reference Data Set
RTD	Resistance Temperature Detector
SA	Sub-Assembly
SCCRED	Standardized and Consolidated Calculated & Reference Experimental Database
SFR	Sodium Fast Reactor
SHRT	Shutdown Heat Removal Test
SM	Simulation Model
SMR	Small Modular Reactor
SYS-TH	System Thermal–Hydraulic
PIOTA	Proximity Instrumented Open Test Assembly
TH	Thermal–Hydraulic
VR	Validation Report
WP	Work Package

Author details

Domenico De Luca[1*], Simone Di Pasquale[1], Marco Cherubini[1], Alessandro Petruzzi[1] and Gianni Bruna[1,2]

1 Nuclear and Industrial Engineering (NINE), Lucca, Italy

2 NucAdvisor, Courbevoie, France

*Address all correspondence to: d.deluca@nineeng.com

IntechOpen

References

[1] Faudon V. Relocaliser en décarbonant grâce à l'énergie nucléaire. Fondation pour l'Innovation Politique, fondapol. org, janvier 2021.

[2] Baroni M. Energie nucléaire: la nouvelle donne international. Fondation pour l'Innovation Politique, fondapol. org, février 2021.

[3] Bruna GB, Apostolakis G., Yasui M., Diaz N., in Buongiorno J., Near - and long-term Regulatory Changes after Fukushima: Does the Accident in Japan call for a Major Overhaul of Nuclear safety Regulations, Embedded Topical Meeting, ANS Winter Meeting, San Diego, California, 11-15 November 2012.

[4] IAEA. Technical Meeting on the Benefits and Challenges of Fast Reactors of the SMR Type. Milan, Italy, 24-27 September 2019.

[5] Commissariat à l'énergie atomique et aux énergies alternatives. Les réacteurs nucléaires à caloporteur sodium. Ed. LeMoniteur, Paris, October 2014.

[6] Bruna GB, et al. Advanced Numerical Simulation and Safety Demonstration. In Numerical Simulations - Applications, Examples and Theory, INTECH, 2011.

[7] IAEA. Benchmark Analysis of EBR-II Shutdown Heat Removal Tests. IAEA-TECDOC-1819, IAEA, Vienna 2017.

[8] Planchon HP, et al. The Experimental Breeder Reactor II Inherent Shutdown Heat Removal Tests – Results and Analysis. Nuclear Engineering and Design, 91(1986) 287-296, 1985.

[9] Petruzzi A, D'Auria F. Standardized Consolidated Calculated and Reference Experimental Database (SCCRED): a Supporting Tool for V&V and Uncertainty Evaluation of Best-Estimate System Codes for Licensing Applications. Nucl. Sci. Eng., 182(1). 2016. pp. 13-53.

[10] Petruzzi A, Giannotti W, Modro M. NEMM - NINE Evaluation Model Methodology. NURETH-18, Portland OR, USNRC, 18-23 August 2019.

[11] Petruzzi A, D'Auria F. Accuracy Quantification: Description of the Fast Fourier Transform Based Method (FFTBM). 3D S.UN.COP., Barcelona, Spain, 7-25 October 2013.

[12] Sumner T, Wei TYC. Benchmark Specifications and Data Requirements for EBR-II Shutdown Heat Removal Tests SHRT-17 and SHRT-45R. ANL-ARC-226 (rev 1), May 31, 2012.

[13] Sumner T. Benchmark Analysis of Fast Flux Test Facility (FFTF) Loss of Flow Without Scram Test. IAEA CRP-I332011. ANL, USA, 2018.

[14] Huo H. Technical Specsifications for Neutronics Benchmark of CEFR Start-up Tests. IAEA CRP-I31032. CIAE, Beijing, 2019.

[15] Leppänen J, et al. The Serpent Monte Carlo code: Status, development and applications in 2013. Ann. Nucl. Energy, 82. 2015, 142-150.

[16] Brown DA, et al. ENDF/B-VIII.0: The 8th Major Release of the Nuclear Reaction Data Library with CIELO-project Cross Sections, New Standards and Thermal Scattering Data. Nuclear Data Sheets, 148. 2018, 1-142.

[17] Chadwick MB, et al. ENDF/B-VII.1 Nuclear Data for Science and Technology: Cross Sections, Covariances, Fission Product Yields and Decay Data. Nuclear Data Sheets, 112. 2011, p. 2887-2996.

[18] Di Pasquale S., Petruzzi A., Giusti V., NINE/UNIPI Final Results, Presentation at the 3rd RCM of the IAEA CRP I31032 on Neutronics Benchmark of CEFR Start-up Tests, April 2021, Virtual Meeting (2021)

[19] Khalil H. Modeling and Simulation Needs for Future Generation Reactors. Joint International Topical Meeting on Mathematics & Computation and Supercomputing in Nuclear Applications (M&C + SNA 2007) Monterey, California, April 15-19, 2007, on CD-ROM, American Nuclear Society, LaGrange Park, IL, 2007.

[20] Cheng SK, Todreas NE. Hydrodynamic models and correlations for bare and wire-wrapped hexagonal rod bundles – bundle friction factors, subchannel friction factors, and mixing parameters. Nuclear Engineering and Design 92. 1986, p. 227-251.

[21] Tenchine D, et al. Status of CATHARE code for sodium cooled fast reactors. Nuclear Engineering and Design 245. 2012, p. 140-152.

[22] Delchini MO, et al. Assessment of SFR Wire Wrap Simulation Uncertainties. ORNL/TM-2016/540, 2016.

[23] Nguyen T, et al. PIV measurements of turbulent flows in a 61-pin wire-wrapped hexagonal fuel bundle. International Journal of Heat and Fluid Flow, 65. 2017, 47-59.

[24] Vaghetto R, et al. Pressure Measurements in a Wire-Wrapped 61-Pin Hexagonal Fuel Bundle. Journal of Fluids Engineering, 140. 2018.